JACS
JOURNAL OF THE AMERICAN CHEMICAL SOCIETY
pubs.acs.org/JACS
Article

The Loss of Interfacial Water-Adsorbate Hydrogen Bond Connectivity Position Surface-Active Hydrogen as a Crucial Intermediate to Enhance Nitrate Reduction Reaction

Shisheng Zheng,* Xinzhe Yang, Zhong-Zhang Shi, Haowen Ding, Feng Pan,* and Jian-Feng Li*

Cite This: J. Am. Chem. Soc. 2024, 146, 26965−26974
Read Online
ACCESS | Metrics & More | Article Recommendations | Supporting Information

ABSTRACT: The electrochemical nitrate reduction reaction (NO_3RR) offers a promising solution for remediating nitrate-polluted wastewater while enabling the sustainable production of ammonia. The control strategy of surface-active hydrogen (*H) is extensively employed to enhance the kinetics of the NO_3RR, but atomic understanding lags far behind the experimental observations. Here, we decipher the cation-water-adsorbate interactions in regulating the NO_3RR kinetics at the Cu (111) electrode/electrolyte interface using AIMD simulations with a slow-growth approach. We demonstrate that the key oxygen-containing intermediates of the NO_3RR (e.g., *NO, *NO_2, and *NO_3) will stably coordinate with the cations, impeding their integration with the hydrogen bond network and further their hydrogenation by interfacial water molecules due to steric hindrance. The *H can migrate across the interface with a low energy barrier, and its hydrogenation barrier with oxygen-containing species remains unaffected by cations, offering a potent supplement to the hydrogenation process, playing the predominant factor by which the *H facilitates NO_3RR reaction kinetic. This study provides valuable insights for understanding the reaction mechanism of NO_3RR by fully considering the cation−water−adsorbate interactions, which can aid in the further development of the electrolyte and electrocatalysts for efficient NO_3RR.

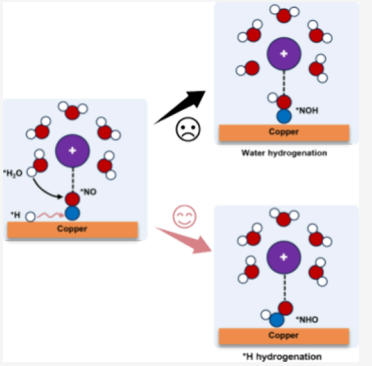

INTRODUCTION

Nitrate (NO_3^-) contamination, arising from the leaching of various sources into the soil, is a widespread issue impacting both surface water and groundwater and finally threatening both human and environmental health.[1] These factors create a strong drive to seek out effective methods for nitrate removal. Traditional biochemical denitrification methods frequently prove ineffective, as they demand harsh conditions and generate large amounts of sludge.[2] Due to the mild conditions and high efficiency, the electrocatalytic reduction of nitrates (NO_3RR) has thus drawn widespread attention.[3−6] Among the various potential products, NH_3 is the most pragmatic, as it is an essential raw material for producing nitrogen fertilizers, fibers, and more. Additionally, its production via the traditional Haber−Bosch process consumes 1% of the world's energy annually.[7−9]

Given that the NO_3RR operates in aqueous solutions, the hydrogen evolution reaction (HER) emerges as the inevitable competing process, serving as the primary factor constraining both the yield rate and the Faradaic efficiency of NH_3.[10,11] The hydrogen evolution reaction (HER) process involves the generation of surface-active hydrogen (*H), also named as Volmer step, and the following Heyrovsky step and/or Tafel step to produce H_2.[12,13] A higher interfacial density of *H often consequently leads to more severe HER. Intriguingly, the generation of *H is also experimentally considered to be an important regulatory strategy that promotes the reduction activity of NO_3RR. Zhao et al. demonstrated a NiFe-layered double hydroxide active phase on an iron surface, with abundant *H participating in the NO_3RR, achieving 90.3% ammonia selectivity. The scavenger of *H by *tert*-butanol obviously weakened the reaction kinetic.[14] Similar results have been reported on S-doped Cu,[15] CeO_x-Modified Cu,[16] Ni_1Cu catalysts,[17] and so on.[5,18−22] It is worth noting that the regulatory role of *H in governing reactions has also garnered significant attention across diverse electrocatalytic processes,[23] encompassing CO_2 electroreduction (CO_2RR),[24−29] oxygen reduction reaction (ORR),[30,31] and nitrogen fixation (NRR).[32−35]

In a word, while the build-up and self-aggregation of H* are the main contributors to HER, they also play a crucial role in steering the kinetic of NO_3RR. The overall reaction pathway of NO_3RR encompasses several intermediates and a multistep hydrogenation process. For each intermediate *M, the hydrogenation process includes two potential modes: one

Received: June 19, 2024
Revised: September 13, 2024
Accepted: September 13, 2024
Published: September 20, 2024

https://doi.org/10.1021/jacs.4c08256
J. Am. Chem. Soc. 2024, 146, 26965−26974

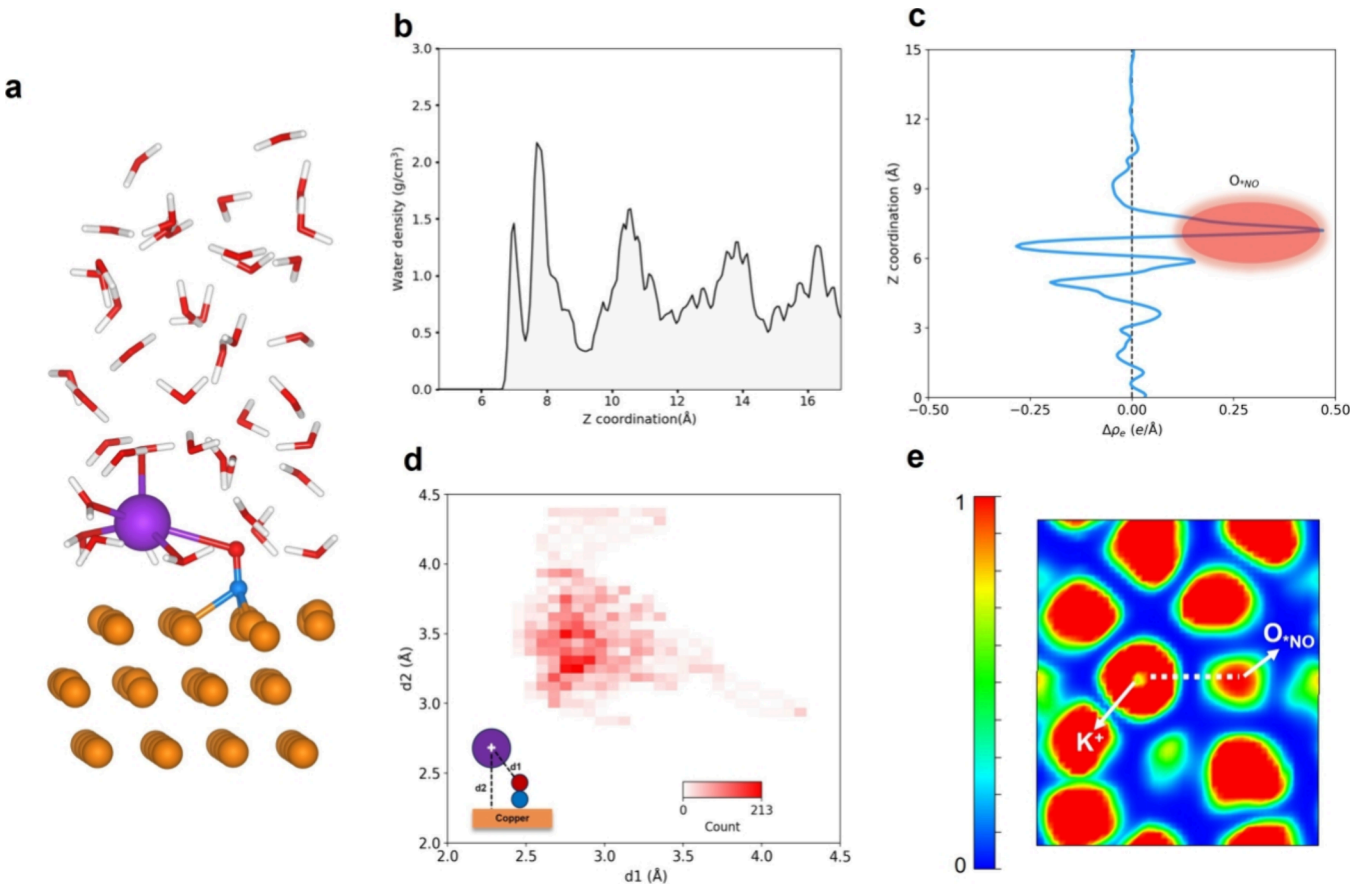

Figure 1. Adsorption configuration of *NO with one K^+ at the interface. (a) Scheme model of *NO adsorption on the Cu electrolyte/electrode interface. (b) Water density along the z direction. The x axis begins from the top layer of copper. (c) Planar-averaged differential charge density of *NO adsorption. $\Delta\rho_e = \rho_{Cu+NO+wat} - \rho_{Cu+wat} - \rho_{NO}$ (d) Statistical results of the distances between the K^+ cation and the interface, as well as between the K^+ cation and oxygen in *NO. The duration of the statistics is 10 ps. (e) ELF analysis of the interactions between *NO and the K^+ cation. The color scale assigns the nondimensional ELF index, where red areas indicate pronounced electron localization. In contrast, blue areas indicate electrons that are delocalized or regions characterized by very low electron density. Color code: Cu, brown; O, red; H, white; N, blue; K purple.

involves the Eley−Rideal (ER) mechanism directly interacting with the H_2O ($*M + H_2O + e^- = *MH + OH^-$), while the other follows the Langmuir−Hinshelwood (LH) mechanisms via *H ($*M + *H = *MH$).[18,36,37] The activation of oxygen-containing species (*NO, $*NO_2$, and $*NO_3$) is often regarded as the crucial step in NO_3RR.[38−40] Certain DFT results proposed that *H can effectively promote these steps through thermodynamic calculations.[15,17,19,21] Nonetheless, these studies often overlook the interfacial solution environment, especially the main components of interfacial water and cations, thereby offering only limited insights. In an aqueous environment, these oxygen-containing species readily integrate into the hydrogen bond network formed by interfacial water, theoretically facilitating the reduction of NO_x via the ER mechanism rather than the LH mechanism involving *H participation. The coordination of cations with intermediate may also influence the reaction kinetics, as proved in many other electrochemical processes.[41−47] Thus, despite the extensive use of the *H regulation strategy to improve the activity of NO_3RR, how it precisely promotes NO_3RR at the microscopic level remains a mystery, in particular, how do interfacial water molecules influence the feasibility of the ER and LH mechanisms? How is the competition between the LH mechanism and HER? What role do cations play in this process? These conceptual deficiencies significantly impede the understanding of the NO_3RR mechanism and rational design of corresponding electrocatalysts.

In this work, we theoretically decipher cation-water-adsorbate interactions in the NO_3RR at the Cu (111) electrode/electrolyte interface using ab initio molecular dynamics (AIMD) simulations with a slow-growth approach. The *NO hydrogenation, a key step in the NO_3RR, is investigated as a protocol to gain atomic insights. We demonstrated that the cation will steadily coordinate with the *NO due to its anionic characteristic, repelling the surrounding interfacial water molecules, thereby hindering the integration of *NO into the interfacial hydrogen bond network and leading to a marked elevation in the energy barrier of the ER mechanism. In contrast, *H generated from interfacial water dissociation can migrate across the interface with a low energy barrier, facilitating the progress of the LH mechanism and suppressing the HER. This conclusion is generalized to $*NO_3$ and $*NO_2$ intermediates. The limitation of the LH mechanism primarily depends on the generation of *H, thus explaining the widespread phenomenon observed in experiments where accelerating water dissociation enhances NO_3RR. Based on these, we predict TiCu and CrCu single-atom copper alloys as effective NO_3RR electrocatalysts. Collectively, we demonstrate a complete atomic mechanism of the cation-water-adsorbate interactions in the electrochemical NO_3RR.

https://doi.org/10.1021/jacs.4c08256
J. Am. Chem. Soc. 2024, 146, 26965−26974

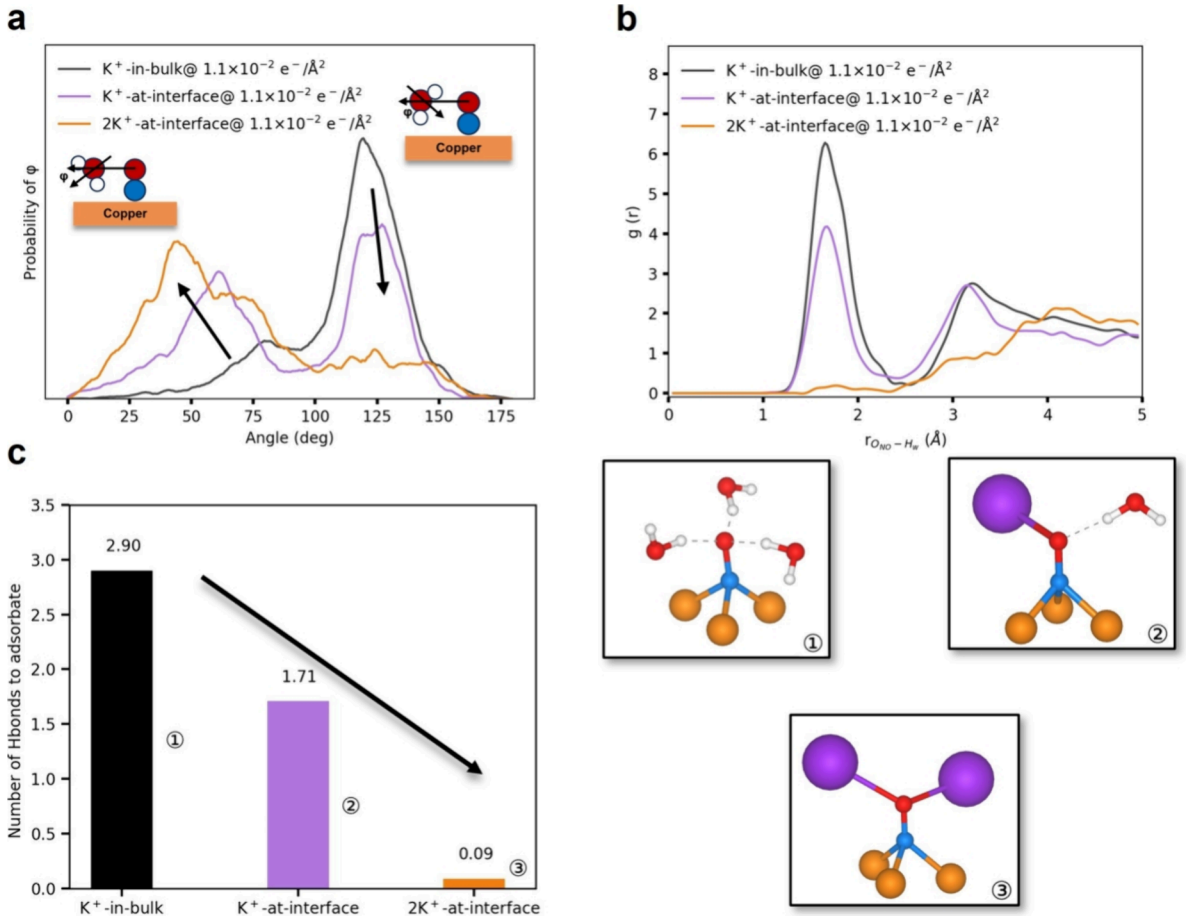

Figure 2. Analysis of interfacial water configuration and hydrogen bond connectivity. (a) Probability distributions of the angle between the vector formed by the oxygen in *NO and the oxygen in water and the bisector of the water, named φ. (b) Radial distribution functions (RDFs) between the O atoms of *NO and the H atoms of water. (c) The average number of hydrogen bonds associated with the *NO in different models throughout the simulation period. The criteria for hydrogen bonds are as follows: O−H−O angles >140° between an oxygen atom of the adsorbate and a water molecule coordinating the former, with the distance between them <3.5 Å.[60] The typical local structures around the *NO are presented. The dashed lines indicate the hydrogen bonds. Color code: Cu, brown; O, red; H, white; N, blue; K purple.

COMPUTATIONAL DETAILS

Copper is widely recognized as an excellent catalyst for NO_3RR.[8,9,39,40,48,49] The Cu (111) surface, which is stable and more active under alkaline conditions,[50] is selected as the simulation model. The orthorhombic 8.96 Å × 10.35 Å Cu (111) slab is constructed with a 35 Å vacuum zone along the z direction. 42 water molecules are added to the vacuum zone to simulate the electrode−electrolyte interface. With the introduction of a $K^+ + e^-$ pair and an adsorbed *NO, the interface exhibits a negative charge, yielding an electrode potential of −0.61 V vs RHE (pH = 13), which roughly corresponds to the operating potential for NO_3RR reduction on some copper-based catalysts.[17,48]

All the calculations were carried out using the density functional theory (DFT) by the Vienna ab initio simulation package (VASP) with the projector-augmented-wave (PAW) scheme.[51] The Perdew−Burke−Ernzerhof (PBE) functional was utilized to describe electron exchange-correlation interactions. Empirical Grimme's D3 scheme was employed to account for van der Waals interactions.[52] The AIMD simulations were carried out to investigate the dynamic nature of interfacial water and cations. The slow-growth approach was utilized to obtain the free energy profile for each reaction step with three independent simulations. More details are described in the Supporting Information.

RESULTS AND DISCUSSIONS

The reduction of NO_3^- to NH_3 is a complex multielectron process, involving numerous potential intermediate species. *NO_3, *NO_2, and *NO are widely regarded as the most important intermediates in this process.[11] Prior research suggested the hydrogenation of *NO is the plausible rate-determining step on copper.[48,49,53] Therefore, we commence our investigation with the analysis of the O-end adsorption structure of *NO with one K^+ at the interface, namely, the "K^+-at-interface" model, as illustrated in Figure 1a. The N-end and side-on adsorption structures are thermodynamically unstable and, thus, are not considered (Figure S3). The distribution of interfacial water was first analyzed (Figure 1b). A distinct water peak is followed by an H-bond gap and then the water density stabilizes around 1 g/cm^3, similar to typical metal/water interfaces.[54,55] This indicates that *NO adsorption does not significantly alter the interfacial water distribution along the z direction. Partial surface charges will populate the antibonding orbitals of *NO. The accumulation of charges on oxygen, as evidenced by the differential charge density (Figure 1c), induces a pronounced anionic character of *NO, which can

https://doi.org/10.1021/jacs.4c08256
J. Am. Chem. Soc. 2024, 146, 26965−26974

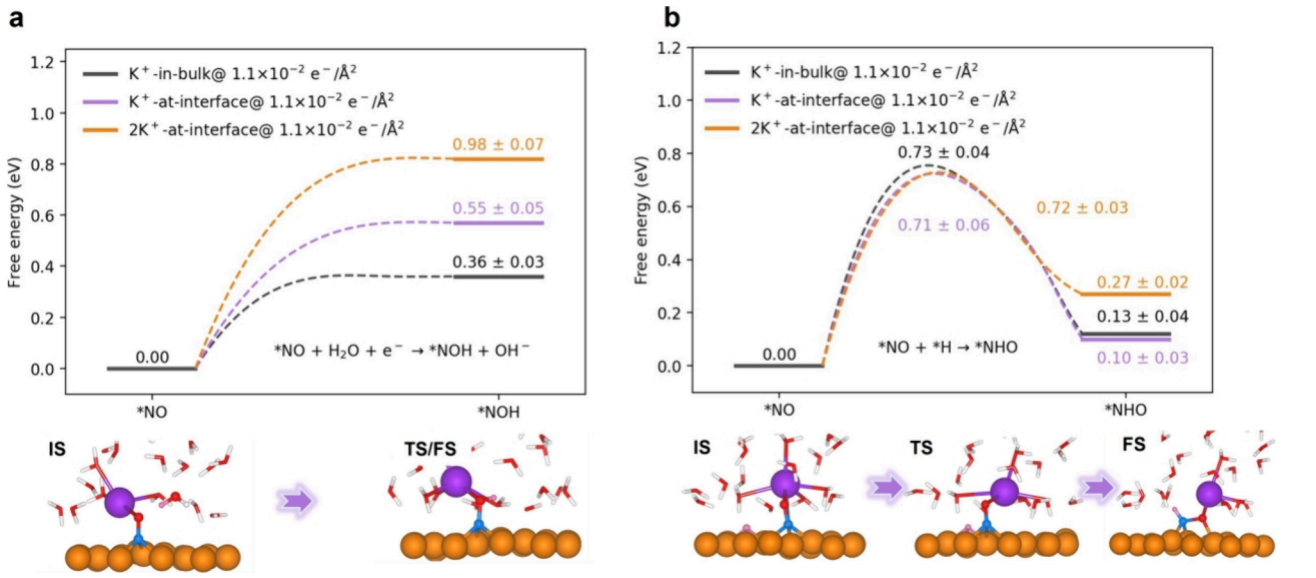

Figure 3. Free energy for *NO hydrogenation. (a) Free energy diagram of *NO hydrogenation to *NOH by the ER mechanism with different models. The typical initial state and transition/final local structures of K^+-at-interface are presented. The transition and final states are quite similar and thus only exampled by one structure. (b) Free energy diagram of *NO hydrogenation to *NHO by the LH mechanism with different models. The typical initial, transition, and final local structures of K^+-at-interface are presented. The dotted line is used to indicate the value of the energy barrier. Color code: Cu, brown; O, red; H, white; N, blue; K purple; H proceeding the reaction, pink.

exert strong electrostatic attraction to the K^+ cation. Combined with the electrostatic force from the negatively charged surface, which helps to confine K^+ near the interface (Figure S1), the K^+ will coordinate with the *NO. Figure 1d presents the statistical results of the distances between the K^+ cation and the interface, as well as between the K^+ cation and oxygen in *NO. It can be observed that for the majority of the simulation time, K^+ cation remains quite close to the interface without exhibiting a tendency to diffuse into the bulk solution. Additionally, stable coordination is achieved between the K^+ cation and the oxygen of *NO, with the distance almost always less than 3.5 Å. The ELF analysis (Figure 1e) is further performed to confirm that the interaction between *NO and K^+ is mainly mediated by a short-range electrostatic interaction between the negative (oxygen) and positive charge (K^+) centers. To quantify the interaction strength between K^+ and *NO, we employed the slow-growth method to calculate the energy required for the detachment of K^+ from *NO, revealing that the process necessitates overcoming an energy barrier of approximately 0.30 eV (Figure S4). If the K^+ cation is placed at a distance of 5 Å from *NO, it can spontaneously escape the solvated water cage and coordinate with *NO within several picoseconds (Figure S5). Introducing a *OH at the interface, which is possible in an alkaline environment, will not affect the coordination between K^+ and *NO (Figure S6). Adjusting the electrode potential by the constant potential method[56,57] also does not affect the coordination of K^+ and *NO (Figure S7). The findings above indicate that the interaction between K^+ and oxygen in *NO is stronger than that between water and oxygen in *NO. The oxygen in *NO can readily integrate into the solvation shell of K^+, forming a stable cation-adsorbate local unit.

The hydrogenation of *NO can proceed via either the ER mechanism or the LH mechanism, with the ER mechanism being directly related to the configuration and distribution of interfacial water. The oxygen in *NO exhibits anionic properties, enabling it to form hydrogen bonds with the interfacial water. If *NO integrates into the hydrogen-bond network formed by interfacial water, it will be in closer spatial proximity to protons in water, facilitating the formation of *NOH. However, K^+ cation forms stable coordination with *NO, which would exert a strong interaction on the distribution of surrounding interfacial water due to its electrostatic force. To investigate the impact of cation coordination on the configuration of interfacial water, we introduce the "K^+-in-bulk" model in which K^+ is placed in the bulk solution, maintaining a distance greater than 10 Å from the interface. This ensures that K^+ has no direct influence on the interface and *NO but can still charge the system (Figure S8). Under actual electrochemical conditions, there could be a significant presence of cations at the interface.[58] We introduce two K^+ cations while maintaining the interface charge density unchanged by double the unit cell area to simulate this scenario, namely, the "$2K^+$-at-interface" model. Two K+ cations will both coordinate with the *NO (Figure S9). The distribution of the angle between the vector formed by the oxygen in *NO and the oxygen in the water and the bisector of the water (φ) is then statistically analyzed (Figure 2a). The results demonstrate that when K^+ is positioned in the bulk solution, the distribution of φ is predominantly centered around 125°. This implies that the OH bonds of water molecules adjacent to *NO are directly oriented toward *NO, thereby promoting hydrogen bond formation with *NO. However, upon coordination between the K^+ cation and *NO, the distribution of φ exhibits a prominent peak at 60°, accompanied by a noticeable reduction in the peak intensity at 125°. The greater the number of K^+ cations, the more pronounced the peak at 60° becomes. This indicates that partial OH bonds of water molecules adjacent to *NO are oriented away from *NO due to the solvation effect of K^+, thereby hindering the formation of hydrogen bonds with *NO. The radial distribution function and hydrogen bond statistics quantified the above conclusions (Figure 2b,c). When K^+ does not coordinate with *NO, the anionic properties of oxygen will

https://doi.org/10.1021/jacs.4c08256
J. Am. Chem. Soc. 2024, 146, 26965−26974

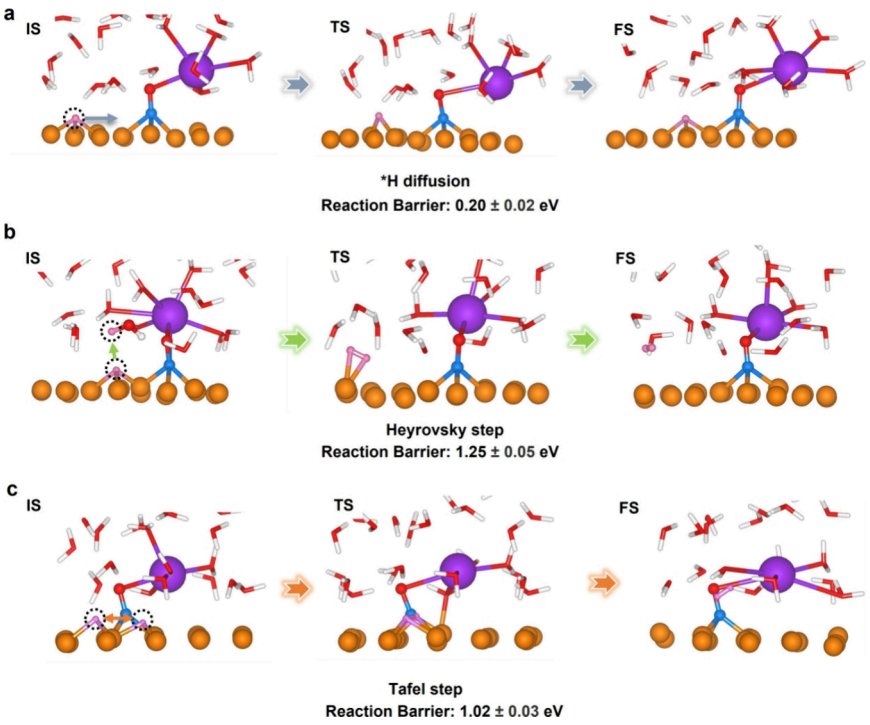

Figure 4. Diffusion of *H and the generation of $*H_2$. (a) Representative structures of initial, transition, and final state of *H diffusion and corresponding reaction barrier. (b) Representative structures of initial, transition, and final state of Heyrovsky step and corresponding reaction barrier. (c) Representative structures of initial, transition, and final state of Tafel step and corresponding reaction barrier. For the sake of clarity, only the surface copper atoms are shown. Color code: Cu, brown; O, red; H, white; N, blue; K purple; H proceed the reaction, pink.

attract a large number of protons around it, resulting in an average of 2.90 hydrogen bonds being formed. In contrast, when one K^+ coordinates with *NO, the number of protons in the first solvation shell of *NO significantly decreases, on average forming 1.71 hydrogen bonds. The number of hydrogen bonds further decreases to 0.09 when *NO coordinates with two K^+ cations. Summarily, the coordination of K^+ with *NO distinctly influences the configuration of interfacial water, rendering it less inclined to approach *NO and establishing a hydrophobic microenvironment around *NO. Experimentally confirming the number of hydrogen bonds may be achieved by the in situ spectroscopy technology.[47,59]

Based on these qualitative understandings, the typical interfacial water molecules around the *NO are selected for evaluating the kinetic barrier of *NO hydrogenation to *NOH via the ER mechanism ($*NO + H_2O + e^- = NOH + OH^-$). The computational results indicate that when K^+ cations are not coordinated with *NO, the energy barrier for the reaction is only 0.36 eV due to the abundant hydrogen bond network connectivity. However, when one K^+ cation coordinates with *NO, the hydrogenation process is apparently hindered, leading to an increased energy barrier of 0.55 eV for *NOH formation (Figure 3a and Figure S10). The activation energy for *NO hydrogenation to *NOH via the ER mechanism will dramatically increase to 0.98 eV with two K^+ coordination due to the almost complete loss of water-adsorbate hydrogen bond connectivity. The aforementioned findings suggest that the coordination of the K^+ cation renders the ER mechanism challenging, thereby leaving room for the LH mechanism to proceed. Through the insertion of a surface *H at the interface near the *NO, we calculated the energy variation for the LH mechanism of *NO hydrogenation to form *NHO (*NO + *H = *NHO). Intriguingly, the coordination of K^+ cation scarcely affects the energy change of this process with reaction barriers consistently around 0.7 eV in different models (Figure 3b and Figure S11), which can be attributed to the small dipole of adsorbed *H atom results in a negligible electric field dependence.[61,62] This also indicates that surface *H can effectively enhance the NO_3RR reaction kinetics, as the activation barrier for the ER mechanism is highly likely to exceed 0.7 eV due to the coordination of interfacial cations. Notably, the formation of *NHO via the ER mechanism ($*NO + H_2O + e^- = *NHO + OH^-$) and the formation of *NOH via the LH mechanism (*NO + *H = *NOH) are both more energetically difficult (Figures S14 and S15) than the previously mentioned pathways and are thus excluded from detailed discussion.

As water molecules pervade the interface, the surface *H may be distant from *NO, requiring *H to freely migrate at the interface, a feasibility confirmed by the remarkably low energy barrier at 0.20 eV (Figure 4a and Figure S16). Additionally, *H may undergo the Heyrovsky reaction ($*H + H_2O + e^- = H_2 + OH^-$) and the Tafel reaction ($*H + *H = H_2$) to produce H_2, which is a major competing reaction in NO_3RR. However, energy calculation results reveal that the energy barriers for these processes are as high as 1.25 and 1.02 eV, respectively (Figure 4b, Figures S17 and S18). As a result, the hydrogen evolution reaction can be inhibited by the fast diffusion of *H and the kinetically unfavorable Heyrovsky and Tafel reaction.

A schematic diagram of cation-water-adsorbate interactions to tune the *NO hydrogenation mode is presented in Figure 5a. In real electrochemical conditions, *NO forms a stable coordination with the K^+ cation, diminishing the connectivity between *NO and the hydrogen bond network. Consequently,

https://doi.org/10.1021/jacs.4c08256
J. Am. Chem. Soc. 2024, 146, 26965−26974

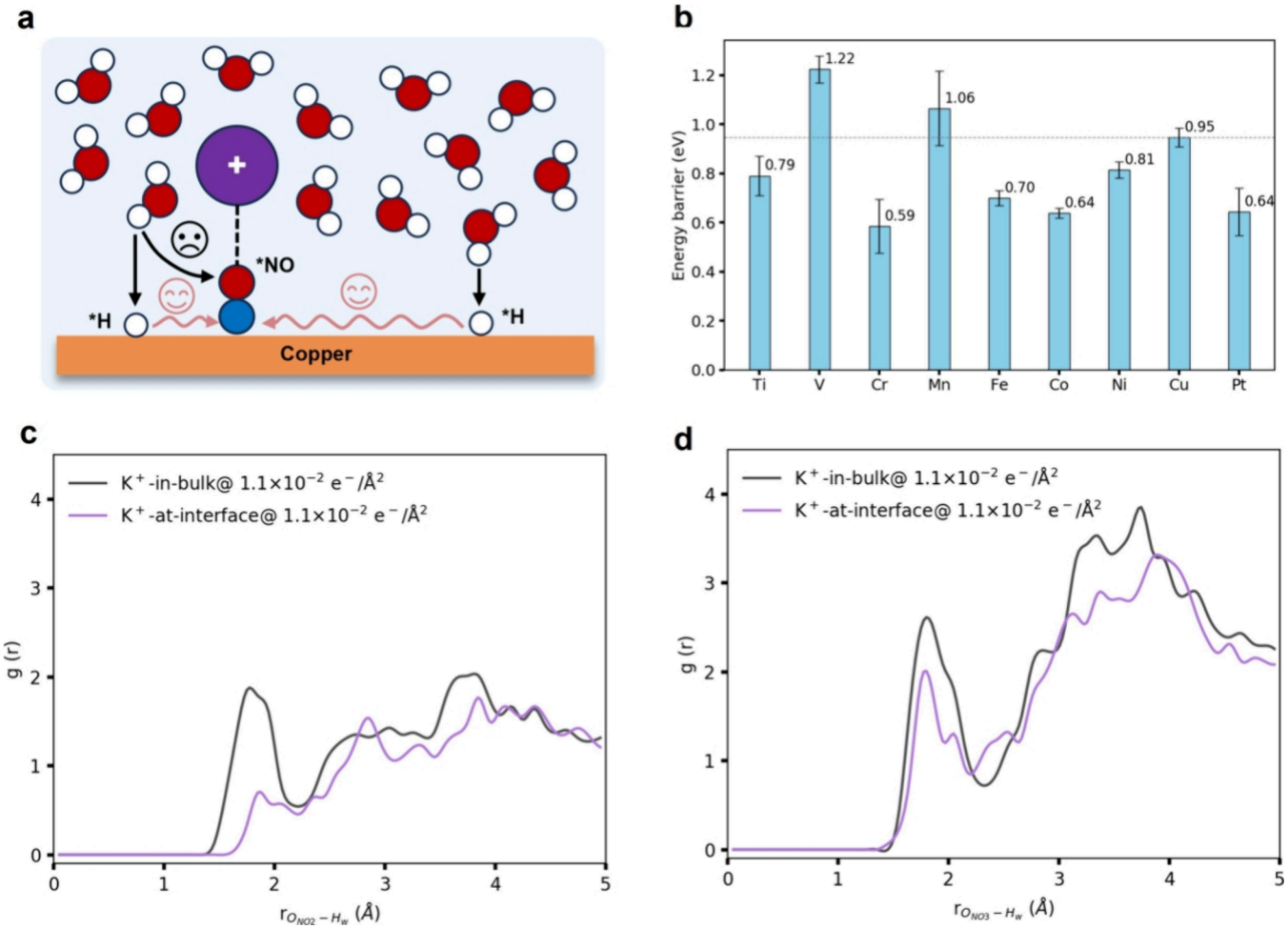

Figure 5. (a) Schematic representation of the atomic mechanism elucidating the role of *H in regulating the NO_3RR reaction kinetics. (b) Energy barrier for the Volmer step on the MCu single atom alloys. The radial distribution functions between the O atoms of (c)*NO_2 and (d) *NO_3 and the H atoms of water.

the energy barrier for the ER mechanism notably escalates. In contrast, surface *H can diffuse across the interface with a low energy barrier, avoiding the formation of hydrogen gas and readily coupling with *NO to form *NHO. In short, the coordination effect of cations impedes water from approaching the adsorbed species while leaving the interfacial hydrogen unaffected, offering a potent supplement to the hydrogenation process of NO_3RR by the surface *H via the LH mechanism, even though the ER mechanism is not completely impossible.

Notably, the LH mechanism can proceed only if surface *H can be formed. In alkaline environments, the generation of *H is primarily achieved through water dissociation, also known as the Volmer process ($H_2O + e^- = *H + OH^-$). The reaction barrier of this step on copper is 0.95 eV (Figure 5b and Figure S19), which implies that the generation of surface *H on pure copper is challenging. The performance of copper for *H generation can also be improved through alloying. Thus, we investigated the kinetic energy barriers for water dissociation on MCu (M = Ti, V, Cr, Mn, Fe, Co, Ni, Pt) single-atom alloys. The results (Figure 5b and Figure S20) show that TiCu, CrCu, FeCu, CoCu, NiCu, and PtCu are more energetically favorable for water dissociation compared to pure copper. Interestingly, FeCu,[63] CoCu,[19,64] NiCu,[17] and PtCu[65] were experimentally reported to accelerate the NO_3RR by *H control strategy, which direct support our hypothesis. The VCu and MnCu undergo the Volmer process with greater difficulty compared to pure copper, and there are no related experimental reports to the best of our knowledge. The TiCu and CrCu are calculated to accelerate hydrolysis and have not yet been experimentally studied, making them promising NO_3RR electrocatalyst candidates. We further investigated the energy barriers for *H diffusion and the Heyrovsky reaction on the Ti and Cr sites. The results show that the generated *H can be easily released from the Ti and Cr sites and diffuse at the interface with an energy barrier of 0.29 and 0.35 eV, respectively (Figure S21), thus accelerating the NO_3RR process on other copper sites, even if themselves may not necessarily serve as an active site for NO_3RR.

Finally, we discuss the universality of the conclusions presented in our work. At the electrochemical interface, cations with strong positive charges are often a major component. When there are centers with strong negative charges, such as the oxygen in *NO, they naturally tend to bind with the cation. Due to the intrinsic solvation capacity, cations exert a repulsive force on hydrogens and an attractive force on oxygens in surrounding water molecules. This organization of local interfacial water molecules hinders the adsorbate from forming hydrogen bonds with them, thereby reducing the efficacy of water as a proton source for hydrogenation. To strengthen our conclusions, we also analyzed the interactions of *NO_2 and

https://doi.org/10.1021/jacs.4c08256
J. Am. Chem. Soc. 2024, 146, 26965−26974

*NO_3—two other key species in the NO_3RR process—with K^+ cation (Figures S22 and S23). The results (Figure S24) show that K^+ forms stable coordination with both of these oxygen-containing species. After coordination, the number of protons surrounding these species significantly decreases (Figure 5c,d). The number of hydrogen bonds connected to *NO_2 decreases from 1.84 when K^+ is in the bulk solution to 0.72 when it is coordinated, and the number of hydrogen bonds connected to *NO_3 decreases from 1.77 in the bulk solution to 0.89 upon coordination. It can be expected that the energy required for hydrogenation of these two species via the ER mechanism will also uphill due to cation coordination. Thus, the surface *H holds the potential to accelerate the hydrogenation of these two species and boost the overall reaction kinetics of NO_3RR. The lack of oxygen in the intermediate, such as *NH_2, actually cannot coordinate with the K^+ cation (Figure S25). The introduction of H_3O^+ to mimic acid conditions does not alter the coordination between the K^+ and *NO (Figure S26), which implies the proposed mechanism may also be applicable under acid conditions.[66,67] Different sizes of cations (Li^+,K^+, and Cs^+) can coordinate with *NO, but large-sized cations will repel more interfacial water molecules due to their space-occupying effect, resulting in fewer hydrogen bonds formed on *NO and may impede the hydrogenation kinetic via ER mechanism (Figure S27).

The surface *H regulatory strategy is also widely employed by experiments in the field of CO_2RR with the potential mechanisms still not fully elucidated.[23,24,26,27,68] For example, Yu and co-workers developed a tandem catalyst by integrating a Cu−S_1N_3 site with Cu clusters.[26] The Cu clusters in the vicinity of Cu−S_1N_3 accelerated the water dissociation and thus provided *H for *CO_2 protonation.[26] This could perhaps be explained by the mechanisms that we proposed. When CO_2 is adsorbed, it is believed to coordinate with cations,[42−44] which may inhibit its ability to undergo the ER mechanism due to its unfeasibility to approach the water molecules. Therefore, active hydrogen can assist in the hydrogenation of CO_2 through the LH mechanism. Based on the above analysis, we speculate that the mechanisms we demonstrated may be pervasive in the field of electrocatalysis. This study also highlights the importance of considering the suitability of alkali metal cations as electrolytes in electrocatalytic hydrogenation processes. While certain species' activation may depend on cation coordination, this coordination is inherently incompatible with interactions between intermediates and protons in interfacial water, illustrating the inherent duality of cations as local charge centers. Achieving the optimal balance between these two aspects is crucial for maximizing both activity and selectivity. The adoption of electronically delocalized chain-like molecules as electrolytes can facilitate the progression of reactions when alkali metal cations are not necessarily required for activating intermediates, as demonstrated in CO reduction.[69] In the present work, we have mainly focused on the cation-tuning effect on the interfacial water. Subsequent research endeavors will delve into whether the presence of cations facilitates specific steps in NO_3RR, akin to CO_2 activation in CO_2 reduction,[42−44] as well as explore the cation effect on the proton transport in the hydrogen bond network.[54,70]

In conclusion, we have investigated the microscopic mechanisms of cation-water-adsorbate interactions in regulating NO_3RR kinetics at the Cu (111) electrode/electrolyte interface using AIMD simulations with a slow-growth approach. We have revealed that the cations will coordinate with oxygen-containing species (e.g., *NO, *NO_2, and *NO_3), hindering their incorporation into the interfacial hydrogen bond network, thereby obstructing their hydrogenation through the ER mechanism. Surface-active hydrogen, however, can migrate across the interface with a low energy barrier, and its hydrogenation barrier with oxygen-containing species via LH mechanism remains unaffected by cations, as demonstrated by *NO hydrogenation. Thus, it becomes a favorable pathway for enhancing reaction kinetics. The LH mechanism is primarily limited by interfacial water dissociation, and TiCu and CrCu single-atom alloys are predicted to effectively accelerate this process. We propose a new mechanism for the understanding of the surface hydrogen-promoting effect by comprehensively considering the cation-water-adsorbate interactions at the atomic level, which provides useful insights into the rational design of NO_3RR electrocatalysts with desirable activity.

■ ASSOCIATED CONTENT

Data Availability Statement

All data are available in the main manuscript or the Supporting Information.

Supporting Information

The Supporting Information is available free of charge at https://pubs.acs.org/doi/10.1021/jacs.4c08256.

Additional computational details; visualizations of the structural models; details of free energy calculations; more statistics on $2K^+$-at-interface model; more statistics on different type of cations (PDF)

■ AUTHOR INFORMATION

Corresponding Authors

Shisheng Zheng − *State Key Laboratory of Physical Chemistry of Solid Surfaces, iChEM, College of Chemistry and Chemical Engineering, College of Materials, College of Energy, College of Electronic Science and Engineering, College of Physical Science and Technology, Fujian Key Laboratory of Ultrafast Laser Technology and Applications, Xiamen University, Xiamen 361000, China*; Email: zhengss@xmu.edu.cn

Feng Pan − *School of Advanced Materials, Peking University, Shenzhen Graduate School, Shenzhen 518000, China*; orcid.org/0000-0002-8216-1339; Email: panfeng@pkusz.edu.cn

Jian-Feng Li − *State Key Laboratory of Physical Chemistry of Solid Surfaces, iChEM, College of Chemistry and Chemical Engineering, College of Materials, College of Energy, College of Electronic Science and Engineering, College of Physical Science and Technology, Fujian Key Laboratory of Ultrafast Laser Technology and Applications, Xiamen University, Xiamen 361000, China; Innovation Laboratory for Sciences and Technologies of Energy Materials of Fujian Province (IKKEM), Xiamen 361000, China*; orcid.org/0000-0003-1598-6856; Email: Li@xmu.edu.cn

Authors

Xinzhe Yang − *School of Advanced Materials, Peking University, Shenzhen Graduate School, Shenzhen 518000, China*; orcid.org/0009-0008-1921-0629

Zhong-Zhang Shi − *State Key Laboratory of Physical Chemistry of Solid Surfaces, iChEM, College of Chemistry*

and Chemical Engineering, College of Materials, College of Energy, College of Electronic Science and Engineering, College of Physical Science and Technology, Fujian Key Laboratory of Ultrafast Laser Technology and Applications, Xiamen University, Xiamen 361000, China

Haowen Ding − *School of Advanced Materials, Peking University, Shenzhen Graduate School, Shenzhen 518000, China*

Complete contact information is available at: https://pubs.acs.org/10.1021/jacs.4c08256

Notes

The authors declare no competing financial interest.

■ ACKNOWLEDGMENTS

This work was supported by grants from the National Natural Science Foundation of China (22402163,21925404, T2293692, 22021001, 21991151, 22322206, and 22361132532), the National Key Research and Development Program of China (2019YFA0705400 and 2022YFA1503803), and ″111″ Project (B17027), Shenzhen Key Laboratory of New Energy Resources Genome Preparation and Testing (no. ZDSYS201707281026184), Guangdong Key Laboratory of Design and calculation of New Energy Materials (no. 2017B030301013), and International joint Research Center for Electric Vehicle Power Battery and Materials (no. 2015B01015).

■ REFERENCES

(1) Ullah, S.; Wang, S.; Li, C.; Jan, A. U.; Zhan, F.; Sharif, H. M. A.; Liu, Q.; Wang, G. Recent developments in designing Cu-based electrocatalysts and advanced strategies for electrochemical nitrate reduction to ammonia. *J. Environ. Chem. Eng.* **2023**, *11* (5), No. 110927.

(2) Jia, Z.; Feng, T.; Ma, M.; Li, Z.; Tang, L. Emerging Advances in Cu-based electrocatalysts for electrochemical nitrate reduction (NO3RR). *Surf. Interfaces* **2024**, *48*, No. 104294.

(3) Chen, G.-F.; Yuan, Y.; Jiang, H.; Ren, S.-Y.; Ding, L.-X.; Ma, L.; Wu, T.; Lu, J.; Wang, H. Electrochemical reduction of nitrate to ammonia via direct eight-electron transfer using a copper−molecular solid catalyst. *Nat. Energy* **2020**, *5* (8), 605−613.

(4) Chen, F. Y.; Wu, Z. Y.; Gupta, S.; Rivera, D. J.; Lambeets, S. V.; Pecaut, S.; Kim, J. Y. T.; Zhu, P.; Finfrock, Y. Z.; Meira, D. M.; King, G.; Gao, G.; Xu, W.; Cullen, D. A.; Zhou, H.; Han, Y.; Perea, D. E.; Muhich, C. L.; Wang, H. Efficient conversion of low-concentration nitrate sources into ammonia on a Ru-dispersed Cu nanowire electrocatalyst. *Nat. Nanotechnol.* **2022**, *17* (7), 759−767.

(5) Han, S.; Li, H.; Li, T.; Chen, F.; Yang, R.; Yu, Y.; Zhang, B. Ultralow overpotential nitrate reduction to ammonia via a three-step relay mechanism. *Nat. Catal.* **2023**, *6* (5), 402−414.

(6) Yang, J.; Qi, H.; Li, A.; Liu, X.; Yang, X.; Zhang, S.; Zhao, Q.; Jiang, Q.; Su, Y.; Zhang, L.; Li, J.-F.; Tian, Z.-Q.; Liu, W.; Wang, A.; Zhang, T. Potential-Driven Restructuring of Cu Single Atoms to Nanoparticles for Boosting the Electrochemical Reduction of Nitrate to Ammonia. *J. Am. Chem. Soc.* **2022**, *144* (27), 12062−12071.

(7) Zhang, R.; Zhang, S.; Cui, H.; Guo, Y.; Li, N.; Zhi, C. Electrochemical nitrate reduction to ammonia using copper-based electrocatalysts. *Next Energy* **2024**, *4*, No. 100125.

(8) Wang, Y.; Zhou, W.; Jia, R.; Yu, Y.; Zhang, B. Unveiling the Activity Origin of a Copper-based Electrocatalyst for Selective Nitrate Reduction to Ammonia. *Angew. Chem., Int. Ed. Engl.* **2020**, *59* (13), 5350−5354.

(9) Fu, Y.; Wang, S.; Wang, Y.; Wei, P.; Shao, J.; Liu, T.; Wang, G.; Bao, X. Enhancing Electrochemical Nitrate Reduction to Ammonia over Cu Nanosheets via Facet Tandem Catalysis. *Angew. Chem., Int. Ed. Engl.* **2023**, *62* (26), No. e202303327.

(10) Xiong, Y.; Wang, Y.; Zhou, J.; Liu, F.; Hao, F.; Fan, Z. Electrochemical Nitrate Reduction: Ammonia Synthesis and the Beyond. *Adv. Mater.* **2024**, *36* (17), 2304021.

(11) Chen, W.; Yang, X.; Chen, Z.; Ou, Z.; Hu, J.; Xu, Y.; Li, Y.; Ren, X.; Ye, S.; Qiu, J.; Liu, J.; Zhang, Q. Emerging Applications, Developments, Prospects, and Challenges of Electrochemical Nitrate-to-Ammonia Conversion. *Adv. Funct. Mater.* **2023**, *33* (29), 2300512.

(12) Shah, A. H.; Wan, C.; Huang, Y.; Duan, X. Toward Molecular Level Understandings of Hydrogen Evolution Reaction on Platinum Surface. *J. Phys. Chem. C* **2023**, *127* (27), 12841−12848.

(13) Jiang, Y.; Huang, J.; Mao, B.; An, T.; Wang, J.; Cao, M. Inside solid-liquid interfaces: Understanding the influence of the electrical double layer on alkaline hydrogen evolution reaction. *Appl. Catal., B* **2021**, *293*, No. 120220.

(14) Wang, K.; Mao, R.; Liu, R.; Zhang, J.; Zhao, H.; Ran, W.; Zhao, X. Intentional corrosion-induced reconstruction of defective NiFe layered double hydroxide boosts electrocatalytic nitrate reduction to ammonia. *Nat. Water* **2023**, *1* (12), 1068−1078.

(15) Xu, Y.; Cheng, C.; Zhu, J.; Zhang, B.; Wang, Y.; Yu, Y. Sulphur-Boosted Active Hydrogen on Copper for Enhanced Electrocatalytic Nitrate-to-Ammonia Selectivity. *Angew. Chem., Int. Ed. Engl.* **2024**, *63* (16), No. e202400289.

(16) Li, Y.; Wang, C.; Yang, L.; Ge, W.; Shen, J.; Zhu, Y.; Li, C. Enhancement of Nitrate-to-Ammonia on Amorphous CeOx-Modified Cu via Tuning of Active Hydrogen Supply. *Adv. Energy Mater.* **2023**, *14* (7), 2303863.

(17) Liu, K.; Li, H.; Xie, M.; Wang, P.; Jin, Z.; Liu, Y.; Zhou, M.; Li, P.; Yu, G. Thermally Enhanced Relay Electrocatalysis of Nitrate-to-Ammonia Reduction over Single-Atom-Alloy Oxides. *J. Am. Chem. Soc.* **2024**, *146* (11), 7779−7790.

(18) Gan, G.; Hong, G.; Zhang, W. Active Hydrogen for Electrochemical Ammonia Synthesis. *Adv. Funct. Mater.* **2024**, *2*, 2401472.

(19) Zhou, Y.; Duan, R.; Li, H.; Zhao, M.; Ding, C.; Li, C. Boosting Electrocatalytic Nitrate Reduction to Ammonia via Promoting Water Dissociation. *ACS Catal.* **2023**, *13* (16), 10846−10854.

(20) Ni, J.; Yan, J.; Li, F.; Qi, H.; Xu, Q.; Su, C.; Sun, L.; Sun, H.; Ding, J.; Liu, B. Atomic Co—P Catalytic Pair Drives Efficient Electrochemical Nitrate Reduction to Ammonia. *Adv. Energy Mater.* **2024**, 2400065.

(21) Luo, H.; Li, S.; Wu, Z.; Liu, Y.; Luo, W.; Li, W.; Zhang, D.; Chen, J.; Yang, J. Modulating the active hydrogen adsorption on Fe−N interface for boosted electrocatalytic nitrate reduction with ultra-long stability. *Adv. Mater.* **2023**, *35* (46), 2304695.

(22) Luo, S.; Guo, H.; Li, T.; Wu, H.; Zhang, F.; Tang, C.; Chen, G.; Yang, G.; Zhou, Y. Ruthenium-induced hydrolysis effect on Fe2O3 nanoarrays for high-performance electrochemical nitrate reduction to ammonia. *Appl. Catal., B* **2024**, *351*, No. 123967.

(23) Liu, H.; Jia, S.; Wu, L.; He, L.; Sun, X.; Han, B. Active hydrogen-controlled CO2/N2/NOx electroreduction: From mechanism understanding to catalyst design. *Innovation Mater.* **2024**, *2* (1), No. 100058.

(24) Chen, S.; Li, X.; Li, H.; Chen, K.; Luo, T.; Fu, J.; Liu, K.; Wang, Q.; Zhu, M.; Liu, M. Proton Transfer Dynamics-Mediated CO(2) Electroreduction. *ChemSusChem* **2023**, *16* (12), No. e202202251.

(25) Zhang, Z.; Gee, W.; Sautet, P.; Alexandrova, A. N. H and CO Co-Induced Roughening of Cu Surface in CO(2) Electroreduction Conditions. *J. Am. Chem. Soc.* **2024**, *146* (23), 16119−16127.

(26) Chen, D.; Zhang, L. H.; Du, J.; Wang, H.; Guo, J.; Zhan, J.; Li, F.; Yu, F. A Tandem Strategy for Enhancing Electrochemical CO(2) Reduction Activity of Single-Atom Cu-S(1) N(3) Catalysts via Integration with Cu Nanoclusters. *Angew. Chem., Int. Ed. Engl.* **2021**, *60* (45), 24022−24027.

(27) Chen, S.; Li, X.; Kao, C. W.; Luo, T.; Chen, K.; Fu, J.; Ma, C.; Li, H.; Li, M.; Chan, T. S.; Liu, M. Unveiling the Proton-Feeding Effect in Sulfur-Doped Fe-N-C Single-Atom Catalyst for Enhanced CO(2) Electroreduction. *Angew. Chem., Int. Ed. Engl.* **2022**, *61* (32), No. e202206233.

(28) Zheng, S.; Liang, X.; Pan, J.; Hu, K.; Li, S.; Pan, F. Multi-Center Cooperativity Enables Facile C−C Coupling in Electrochemical CO2 Reduction on a Ni2P Catalyst. *ACS Catal.* **2023**, *13* (5), 2847−2856.
(29) Wang, X.; Sang, X.; Dong, C. L.; Yao, S.; Shuai, L.; Lu, J.; Yang, B.; Li, Z.; Lei, L.; Qiu, M.; Dai, L.; Hou, Y. Proton Capture Strategy for Enhancing Electrochemical CO2 Reduction on Atomically Dispersed Metal−Nitrogen Active Sites. *Angew. Chem., Int. Ed. Engl.* **2021**, *60* (21), 11959−11965.
(30) Engstfeld, A. K.; Beckord, S.; Fuchs, S.; Behm, R. J. Impact of the Potential Dependent Surface Adlayer Composition on the ORR Activity and H2O2 Formation on Ru(0001) in Acid Electrolytes. *ChemCatChem* **2024**, No. e202400271.
(31) Mahata, A.; Nair, A. S.; Pathak, B. Recent advancements in Pt-nanostructure-based electrocatalysts for the oxygen reduction reaction. *Catal. Sci. Technol.* **2019**, *9* (18), 4835−4863.
(32) Ling, C.; Zhang, Y.; Li, Q.; Bai, X.; Shi, L.; Wang, J. New Mechanism for N2 Reduction: The Essential Role of Surface Hydrogenation. *J. Am. Chem. Soc.* **2019**, *141* (45), 18264−18270.
(33) Lv, X.; Kou, L.; Frauenheim, T. Hydroxyl-Boosted Nitrogen Reduction Reaction: The Essential Role of Surface Hydrogen in Functionalized MXenes. *ACS Appl. Mater. Interfaces* **2021**, *13* (12), 14283−14290.
(34) Bian, X.; Zhao, Y.; Zhang, S.; Li, D.; Shi, R.; Zhou, C.; Wu, L.-Z.; Zhang, T. Enhancing the Supply of Activated Hydrogen to Promote Photocatalytic Nitrogen Fixation. *ACS Mater. Lett.* **2021**, *3* (11), 1521−1527.
(35) Utomo, W. P.; Leung, M. K. H.; Yin, Z.; Wu, H.; Ng, Y. H. Advancement of Bismuth-Based Materials for Electrocatalytic and Photo(electro)catalytic Ammonia Synthesis. *Adv. Funct. Mater.* **2021**, *32*, 2106713.
(36) Cheng, T.; Xiao, H.; Goddard, W. A., III Full atomistic reaction mechanism with kinetics for CO reduction on Cu(100) from ab initio molecular dynamics free-energy calculations at 298 K. *Proc. Natl. Acad. Sci. U. S. A.* **2017**, *114* (8), 1795−1800.
(37) Wang, Y.; Wang, C.; Li, M.; Yu, Y.; Zhang, B. Nitrate electroreduction: mechanism insight, in situ characterization, performance evaluation, and challenges. *Chem. Soc. Rev.* **2021**, *50* (12), 6720−6733.
(38) Wang, Z.; Richards, D.; Singh, N. Recent discoveries in the reaction mechanism of heterogeneous electrocatalytic nitrate reduction. *Catal. Sci. Technol.* **2021**, *11* (3), 705−725.
(39) Wan, H.; Bagger, A.; Rossmeisl, J. Electrochemical Nitric Oxide Reduction on Metal Surfaces. *Angew. Chem., Int. Ed. Engl.* **2021**, *60* (40), 21966−21972.
(40) Teng, M.; Ye, J.; Wan, C.; He, G.; Chen, H. Research Progress on Cu-Based Catalysts for Electrochemical Nitrate Reduction Reaction to Ammonia. *Ind. Eng. Chem. Res.* **2022**, *61* (40), 14731−14746.
(41) Yang, X.; Ding, H.; Li, S.; Zheng, S.; Li, J.-F.; Pan, F. Cation-Induced Interfacial Hydrophobic Microenvironment Promotes the C−C Coupling in Electrochemical CO2 Reduction. *J. Am. Chem. Soc.* **2024**, *146* (8), 5532−5542.
(42) Monteiro, M. C. O.; Dattila, F.; Hagedoorn, B.; García-Muelas, R.; López, N.; Koper, M. T. M. Absence of CO electroreduction on copper, gold and silver electrodes without metal cations in solution. *Nat. Catal.* **2021**, *4* (8), 654−662.
(43) Zhang, Z.; Li, H.; Shao, Y.; Gan, L.; Kang, F.; Duan, W.; Hansen, H. A.; Li, J. Molecular understanding of the critical role of alkali metal cations in initiating CO(2) electroreduction on Cu(100) surface. *Nat. Commun.* **2024**, *15* (1), 612.
(44) Qin, X.; Vegge, T.; Hansen, H. A. Cation-Coordinated Inner-Sphere CO2 Electroreduction at Au−Water Interfaces. *J. Am. Chem. Soc.* **2023**, *145* (3), 1897−1905.
(45) Kumeda, T.; Laverdure, L.; Honkala, K.; Melander, M. M.; Sakaushi, K. Cations Determine the Mechanism and Selectivity of Alkaline Oxygen Reduction Reaction on Pt(111). *Angew. Chem., Int. Ed. Engl.* **2023**, *62* (51), No. e202312841.
(46) Shin, S. J.; Choi, H.; Ringe, S.; Won, D. H.; Oh, H. S.; Kim, D. H.; Lee, T.; Nam, D. H.; Kim, H.; Choi, C. H. A unifying mechanism for cation effect modulating C1 and C2 productions from CO(2) electroreduction. *Nat. Commun.* **2022**, *13* (1), 5482.
(47) Wang, Y.-H.; Zheng, S.; Yang, W.-M.; Zhou, R.-Y.; He, Q.-F.; Radjenovic, P.; Dong, J.-C.; Li, S.; Zheng, J.; Yang, Z.-L.; Attard, G.; Pan, F.; Tian, Z.-Q.; Li, J.-F. In situ Raman spectroscopy reveals the structure and dissociation of interfacial water. *Nature* **2021**, *600* (7887), 81−85.
(48) Wei, M.; Li, S.; Wang, X.; Zuo, G.; Wang, H.; Meng, X.; Wang, J. A Perspective on Cu-Based Electrocatalysts for Nitrate Reduction for Ammonia Synthesis. *Adv. Energy Sustainability Res.* **2023**, *5* (1), 2300173.
(49) Karamad, M.; Goncalves, T. J.; Jimenez-Villegas, S.; Gates, I. D.; Siahrostami, S. Why copper catalyzes electrochemical reduction of nitrate to ammonia. *Faraday Discuss.* **2023**, *243* (0), 502−519.
(50) Wei, J.; Li, Y.; Lin, H.; Lu, X.; Zhou, C.; Li, Y. Y. Copper-based electro-catalytic nitrate reduction to ammonia from water: Mechanism, preparation, and research directions. *Environ. Sci. Ecotechnology* **2024**, *20*, No. 100383.
(51) Blöchl, P. E. Projector Augmented-Wave Method. *Phys. Rev. B* **1994**, *50* (24), 17953−17979.
(52) Grimme, S.; Antony, J.; Ehrlich, S.; Krieg, H. A consistent and accurate ab initio parametrization of density functional dispersion correction (DFT-D) for the 94 elements H-Pu. *J. Chem. Phys.* **2010**, *132* (15), 154104.
(53) Hu, T.; Wang, C.; Wang, M.; Li, C. M.; Guo, C. Theoretical Insights into Superior Nitrate Reduction to Ammonia Performance of Copper Catalysts. *ACS Catal.* **2021**, 14417−14427.
(54) Li, P.; Jiang, Y.; Hu, Y.; Men, Y.; Liu, Y.; Cai, W.; Chen, S. Hydrogen bond network connectivity in the electric double layer dominates the kinetic pH effect in hydrogen electrocatalysis on Pt. *Nat. Catal.* **2022**, *5* (10), 900−911.
(55) Li, X. Y.; Chen, A.; Yang, X. H.; Zhu, J. X.; Le, J. B.; Cheng, J. Linear Correlation between Water Adsorption Energies and Volta Potential Differences for Metal/water Interfaces. *J. Phys. Chem. Lett.* **2021**, *12* (30), 7299−7304.
(56) Bai, X.; Zhao, X.; Zhang, Y.; Ling, C.; Zhou, Y.; Wang, J.; Liu, Y. Dynamic Stability of Copper Single-Atom Catalysts under Working Conditions. *J. Am. Chem. Soc.* **2022**, *144* (37), 17140−17148.
(57) Zhao, X.; Liu, Y. Origin of Selective Production of Hydrogen Peroxide by Electrochemical Oxygen Reduction. *J. Am. Chem. Soc.* **2021**, *143* (25), 9423−9428.
(58) Garlyyev, B.; Xue, S.; Watzele, S.; Scieszka, D.; Bandarenka, A. S. Influence of the Nature of the Alkali Metal Cations on the Electrical Double-Layer Capacitance of Model Pt(111) and Au(111) Electrodes. *J. Phys. Chem. Lett.* **2018**, *9* (8), 1927−1930.
(59) Li, C. Y.; Le, J. B.; Wang, Y. H.; Chen, S.; Yang, Z. L.; Li, J. F.; Cheng, J.; Tian, Z. Q. In situ probing electrified interfacial water structures at atomically flat surfaces. *Nat. Mater.* **2019**, *18* (7), 697−701.
(60) Heenen, H. H.; Gauthier, J. A.; Kristoffersen, H. H.; Ludwig, T.; Chan, K. Solvation at metal/water interfaces: An ab initio molecular dynamics benchmark of common computational approaches. *J. Chem. Phys.* **2020**, *152* (14), 144703.
(61) Ringe, S.; Clark, E. L.; Resasco, J.; Walton, A.; Seger, B.; Bell, A. T.; Chan, K. Understanding cation effects in electrochemical CO2 reduction. *Energy Environ. Sci.* **2019**, *12* (10), 3001−3014.
(62) Clark, E. L.; Ringe, S.; Tang, M.; Walton, A.; Hahn, C.; Jaramillo, T. F.; Chan, K.; Bell, A. T. Influence of Atomic Surface Structure on the Activity of Ag for the Electrochemical Reduction of CO2 to CO. *ACS Catal.* **2019**, *9* (5), 4006−4014.
(63) Tang, Z.; Bai, Z.; Li, X.; Ding, L.; Zhang, B.; Chang, X. Chloride-Derived Bimetallic Cu-Fe Nanoparticles for High-Selective Nitrate-to-Ammonia Electrochemical Catalysis. *Processes* **2022**, *10* (4), 751.
(64) Fang, J. Y.; Zheng, Q. Z.; Lou, Y. Y.; Zhao, K. M.; Hu, S. N.; Li, G.; Akdim, O.; Huang, X. Y.; Sun, S. G. Ampere-level current density ammonia electrochemical synthesis using CuCo nanosheets simulating nitrite reductase bifunctional nature. *Nat. Commun.* **2022**, *13* (1), 7899.

https://doi.org/10.1021/jacs.4c08256
J. Am. Chem. Soc. 2024, 146, 26965−26974

(65) Kori, D. K. K.; Das, A. K. Engineering of Bimetallic Cu−Pt Nanostructures for the Electrochemical Ammonia Synthesis via Nitrate Reduction. *ACS Appl. Eng. Mater.* **2023**, *1* (9), 2386−2396.
(66) Ba, J.; Dong, H.; Odziomek, M.; Lai, F.; Wang, R.; Han, Y.; Shu, J.; Antonietti, M.; Liu, T.; Yang, W.; Tian, Z. Red Carbon Mediated Formation of Cu(2)O Clusters Dispersed on the Oxocarbon Framework by Fehling's Route and their Use for the Nitrate Electroreduction in Acidic Conditions. *Adv. Mater.* **2024**, *36* (25), 2400396.
(67) Zhang, R.; Li, C.; Cui, H.; Wang, Y.; Zhang, S.; Li, P.; Hou, Y.; Guo, Y.; Liang, G.; Huang, Z.; Peng, C.; Zhi, C. Electrochemical nitrate reduction in acid enables high-efficiency ammonia synthesis and high-voltage pollutes-based fuel cells. *Nat. Commun.* **2023**, *14* (1), 8036.
(68) Feng, J.; Zhang, L.; Liu, S.; Xu, L.; Ma, X.; Tan, X.; Wu, L.; Qian, Q.; Wu, T.; Zhang, J.; Sun, X.; Han, B. Modulating adsorbed hydrogen drives electrochemical CO(2)-to-C(2) products. *Nat. Commun.* **2023**, *14* (1), 4615.
(69) Li, J.; Li, X.; Gunathunge, C. M.; Waegele, M. M. Hydrogen bonding steers the product selectivity of electrocatalytic CO reduction. *Proc. Natl. Acad. Sci. U. S. A.* **2019**, *116* (19), 9220−9229.
(70) Li, X. Y.; Wang, T.; Cai, Y. C.; Meng, Z. D.; Nan, J. W.; Ye, J. Y.; Yi, J.; Zhan, D. P.; Tian, N.; Zhou, Z. Y.; Sun, S. G. Mechanism of Cations Suppressing Proton Diffusion Kinetics for Electrocatalysis. *Angew. Chem., Int. Ed. Engl.* **2023**, *62* (14), No. e202218669.

https://doi.org/10.1021/jacs.4c08256
J. Am. Chem. Soc. 2024, 146, 26965−26974